DIFFERENTIAL INFORMATION CONTENT IN STAGGERED MULTIPLE SHELL HARDI MEASURED BY THE TENSOR DISTRIBUTION FUNCTION

Liang Zhan[1], Alex D. Leow[2, 3], Iman Aganj[4], Christophe Lenglet[5, 4], Guillermo Sapiro[4], Essa Yacoub[5], Noam Harel[5], Arthur W. Toga[1], Paul M. Thompson[1]

[1] Laboratory of Neuro Imaging, Dept. Neurology, UCLA School of Medicine, Los Angeles, CA, USA.
[2] Dept. Psychiatry, Univ. of Illinois-Chicago, IL, USA
[3] Community Psychiatry Associates, Sacramento, CA, USA
[4] Dept. of Electrical and Computer Engineering, Univ. of Minnesota, Minneapolis, MN, USA.
[5] Center for Magnetic Resonance Research, Univ. of Minnesota, Minneapolis, MN, USA

ABSTRACT

Diffusion tensor imaging has accelerated the study of brain connectivity, but single-tensor diffusion models are too simplistic to model fiber crossing and mixing. Hybrid diffusion imaging (HYDI) samples the radial and angular structure of local diffusion on multiple spherical shells in *q*-space, combining the high SNR and CNR achievable at low and high *b*-values, respectively. We acquired and analyzed human multi-shell HARDI at ultra-high field-strength (7 Tesla; *b*=1000, 2000, 3000 s/mm^2). In experiments with the tensor distribution function (TDF), the *b*-value affected the intrinsic uncertainty for estimating component fiber orientations and their diffusion eigenvalues. We computed orientation density functions by least-squares fitting in multiple HARDI shells simultaneously. Within the range examined, higher *b*-values gave improved orientation estimates but poorer eigenvalue estimates; lower *b*-values showed opposite strengths and weaknesses. Combining these strengths, multiple-shell HARDI, especially with staggered angular sampling, outperformed single-shell scanning protocols, even when overall scanning time was held constant.

Index Terms—HARDI, multi-shell, ODF, TDF, Entropy

1. INTRODUCTION

Diffusion-weighted MRI is a powerful tool to study water diffusion in tissue, providing vital information on white matter microstructure, such as fiber connectivity and integrity in the healthy and diseased brain. To date, most clinical studies still employ the *diffusion tensor imaging* (DTI) model [1,2]. This describes the anisotropy of local water diffusion in tissues by estimating, from a set of *K* diffusion-sensitized images, the 3x3 *diffusion tensor* (the covariance matrix of a 3-dimensional Gaussian distribution). Seven independent gradients are mathematically sufficient to determine the diffusion tensor. However, diffusion will not be Gaussian in situations where fibers cross or mix. The tensor model also fails to represent non-mono-exponential diffusion decay (e.g., so-called fast and slow diffusion), and partial volume averaging effects among different tissues (where a single voxel has contributions to diffusion from gray matter, white matter and cerebrospinal fluid). To overcome the limitations of the single-tensor model, a broad spectrum of methods have been proposed.

Some approaches analyze more angular measures at a fixed level of diffusion weighting (the *b*-value). These approaches include high angular resolution diffusion imaging (HARDI) and reconstruction methods such as *q*-ball imaging (QBI) [3], and related deconvolution methods [4]. HARDI signals may also be reconstructed using the diffusion orientation transform (DOT) [5], fields of von Mises-Fisher mixtures [6], or higher-order tensors (i.e., 3x3x…x3 tensors) [7]. Another type of approach, diffusion spectrum imaging (DSI [8]), discretely samples the *q*-space, usually at grid points, and exploits the Fourier relationship to estimate the diffusion PDF without assuming a model. DSI measures the signal using Cartesian sampling and resolves diffusion micro-structures by direct model-free Fourier inversion of the diffusion signal [8]. Even so, DSI can be inefficient as a large number of measurements are required to encode *q*-space at each voxel, which is very time consuming [9]. An alternative approach based on sampling only on multiple spherical shells in the *q*-space has been proposed, referred to as multi-shell high angular resolution diffusion imaging or *hybrid* diffusion imaging (HYDI; [10, 11]). Each spherical shell is a 2D manifold with a fixed *b*-value, and the number of sampling gradients grows quadratically with the desired angular resolution, as opposed to cubically with DSI. A few studies exploit data from multiple shells to simultaneously benefit from the high signal-to-noise ratio (SNR) obtainable at low *b*-values and the high angular contrast-to-noise ratio (CNR) obtainable at high *b*-values [10-12]. Even so, the main barrier in multi-shell HARDI is how to integrate information from different shells. In these studies, a key goal is to more accurately

model the PDF describing the complex water diffusion phenomenon, or at least create new scalar measures that go beyond just the angular information in the diffusion signal to include radial information as well.

The Tensor Distribution Function (TDF) was recently proposed in [13] to model multidirectional diffusion at each point as a probabilistic mixture of symmetric positive definite tensors. The TDF models the diffusion signal more flexibly, as a unit-mass probability density on the 6D manifold of symmetric positive definite tensors. This yields a TDF, or continuous mixture of tensors, at each point in the brain. Using the calculus of variations, the TDF approach separates different dominant fiber directions in each voxel and computes their individual eigenvalues, and anisotropy measures weighted by fiber components. From the TDF, one can derive analytic formulae for the orientation distribution function (ODF), the tensor orientation distribution (TOD), and their corresponding anisotropy measures. In this study, we illustrate (1) how to manipulate multi-shell HARDI data using the TDF, and (2) how to compare the information content of different HYDI sampling schemes.

2. METHODS

2.1 TDF Principle and Implementation

For the diffusion tensor model, both the diffusion probability density function (PDF) and the q-space signal are assumed to be multivariate Gaussian. The diffusion-sensitized MRI signal in gradient direction q is modeled using a simple mono-exponential decay function:

$$S_x = S_0 \cdot \exp\left(-bq^T Dq\right) \quad (1)$$

where S_0 is the non-diffusion-weighted signal intensity; b is the instrumental scaling factor, or level of diffusion weighting, containing information on the pulse sequence, gradient strength, and physical constants, which is unique corresponding to each q-space shell; q is the gradient direction unit vector and q^T denotes vector transpose; D is the diffusion tensor, which is a 3x3 symmetric positive definite matrix. Without loss of generality, let us assume the constant S_0 is 1.

We denote the space of symmetric positive definite three-by-three matrices by $\overline{D}$. The probabilistic ensemble of tensors, as represented by a tensor distribution function (TDF) P, is defined on the tensor space $\overline{D}$ that best explains the observed diffusion-weighted signals[13]:

$$S_{cal}(q) = \int_{D\in\overline{D}} P(D)\exp(-bq^T Dq)\, dD \quad (2)$$

To solve for an optimal TDF P^*, we use the multiple diffusion-sensitized gradient directions q_i and arrive at P* using the least-squares principle with the gradient descent defined in [13]:

$$P^* = argmin_P \sum_i \left(S_{obs}(q_i) - S_{cal}(q_i)\right)^2 \quad (3)$$

By parameterizing the tensor space using eigenvalues (λ) and Euler angles (θ), the dominant fiber direction may be estimated from Eq. 4 using a simple thresholding of the tensor orientation density as a function of spherical angle[13]:

$$TOD(\theta) = \int_\lambda P(D(\lambda,\theta))d\lambda \quad (4)$$

From the TDF, the orientation density function (ODF) [13-15] may be computed analytically, from Eq. 5:

$$ODF(\tilde{x}) = \frac{1}{4\pi}\sum_{D\in\overline{D}} \frac{P(D)}{\det(D)^{\frac{1}{2}}(\tilde{x}^t D^{-1}\tilde{x})^{\frac{3}{2}}} \quad (5)$$

These ODFs were rendered using 642 point samples, determined using an icosahedral approximation of the unit sphere.

Here we estimated TDFs using a multi-resolution strategy. At each new resolution, new unit directions were added (i.e., upsampling) around the maximal values of the TOD with respect to a discretization of the unit sphere. We can repeat this upsampling process to achieve higher and higher resolution, depending on the required angular accuracy.

2.2 Least-squares approach for multi-shell HARDI (multi-shell LS)

If the diffusion-weighted signals were collected from M distinct shells in the q space, and assume each shell uses N gradient directions, with q_{ij} the diffusion-sensitizing gradient vector for the j-th direction in the i-th shell (with a b-value of b_i), then the least-squares approach for fitting a TDF to multi-shell HARDI data can be expressed in Eq. 6:

$$\begin{cases} S_{cal}(q_{ij}) = \int_{D\in\overline{D}} P(D)\exp\left(-b_i {q_{ij}}^T D q_{ij}\right)dD \\ P^* = argmin_P \sum_{i=1}^M w_i \cdot \left[\sum_{j=1}^N (S_{obs}(q_{ij}) - S_{cal}(q_{ij}))^2\right] \\ \sum_{i=1}^M w_i = 1 \end{cases} \quad (6)$$

Here we apply the least-squares approach to extend the definition of the TDF from single shell data to multi-shell diffusion data. In this paper, we will use an equal weighting (w_i=1/M). This is the simplest way to determine the weights, but other ways of weighting may be employed, which we plan to investigate in future studies. In future, adaptive weighting strategy multi-shell HYDI will be investigated.

2.3 Evaluation

To fairly compare multi-shell versus single-shell HARDI scans, it is not sufficient to add new shells with the same angular sampling, as the multi-shell acquisition would contain more measurements. This would automatically increase the signal-to-noise ratio (but it would also lengthen the scan time). To compare sampling schemes that would take the same amount of time to acquire, we sub-sampled each of the M single shells to contain 1/M angular samples. This slightly reduces the angular resolution of each shell. HYDI data were collected at 3 different b-values; each single shell had 256 angular samples, so we created a multi-shell HARDI dataset by sub-sampling one third of the angular samples (85) from each shell. The final multi-shell HARDI will have 255 (=85x3) angular samples if all shells

are combined. Sub-sampling was performed using PDEs based on electrostatic repulsion, that aim to minimize an angular distribution energy [16]. Here we investigated two HYDI sampling schemes: the first uses consistent sampling of the same spherical angles in every shell (named LS Multi-shell-1) and the other scheme uses a staggered sampling (named LS Multi-shell-2). In the staggered sampling, three different subsamples are taken from the three single shells to form the final multi-shell data. **Figure 1** illustrates the sub-sample schedules for two HYDI.

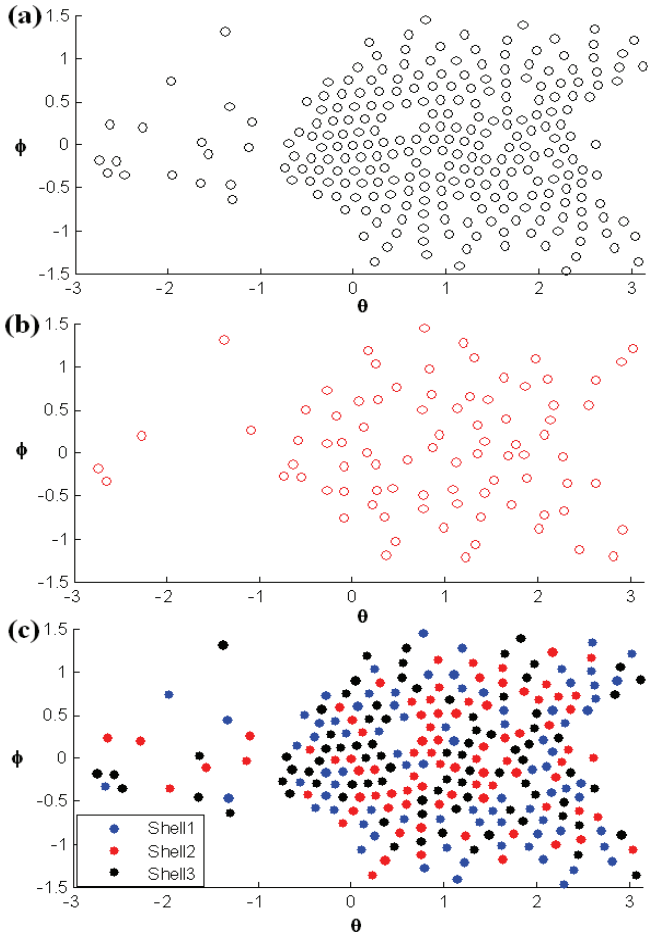

Figure 1. Sampling Schedules for single-shell HARDI, and two sampling methods for multi-shell HYDI. (a) Original angular sampling schedule for one single shell (256 angular points distributed in the spherical surface). (b) This scheme uses the same sub-sampling schedule for all three shells (selecting 85 angular points from the original 256 points by minimizing the angular distribution energy). By sampling these same angles in all 3 shells, we can form the 255-sample multi-shell HYDI dataset. (c) This "staggered" sampling scheme uses different directions in every shell. We sub-sample the data in the three shells, selecting three non-overlapping 85-direction sets from the original 256 points by optimizing the total angular resolution within each shell. We then form a 255-direction multi-shell HYDI dataset, with different directions in every shell [please refer to 16 for more details].

Several parameters may be calculated to evaluate single-shell and multi-shell results. Firstly, the generalized fractional anisotropy (GFA) may be used to evaluate the variation in the ODF with respect to spherical angle. The higher the GFA value is, the more "concentrated" the ODF profile is:

$$GFA \triangleq \sqrt{\frac{n\sum_{i=1}^{n}(ODF(x_i)-<ODF(x_i)>)^2}{[(n-1)\sum_{i=1}^{n}ODF(x_i)^2]}} \quad (7)$$

Here ODF(x_i) in direction x_i is computed from Eq. (5) , <ODF(x_i)> is the mean value of the ODF across all angles, and n is the number of discretized ODF profiles.

While GFA computes the overall anisotropy of the local diffusion profile, we also wanted to investigate whether the *b*-value affects the estimation of the orientations of fiber tracts, versus the estimation of the eigenvalues. To the best of our knowledge, this has not been previously investigated using human HARDI, HYDI or DSI. Due to the probabilistic nature of the TDF method, the concept of Shannon entropy can be easily adapted to our advantage.

To this end, we first form the marginal densities of the angular and eigenvalue components of the voxel-wise TDF (e.g., the angular component of TDF is defined by integrating out the eigenvalue component of TDF); we then compute their respective Shannon entropies. This procedure allows us to remove the influence of the fiber orientation on the uncertainty in estimating its eigenvalues, and *vice versa*. Mathematically, from the voxelwise TDF, we compute (1) the TDF Shannon Entropy (SE) of P^*, which is calculated from Eq. (6); (2) the angular entropy (AE), i.e., the Shannon entropy of P_θ (the angular component of TDF); and (3) the eigenvalue entropy (EE), i.e., the Shannon entropy of P_λ (the eigenvalue component of TDF).

$$\begin{cases} P_\theta = \int_\lambda P^*(D(\lambda,\theta))d\lambda \\ P_\lambda = \int_\theta P^*\big(D(\lambda,\theta)\big)d\theta \\ SE = -\int_D P^* \times \log(P^*)\, dD \\ AE = -\int_\theta P_\theta \times \log(P_\theta)\, d\theta \\ EE = -\int_\lambda P_\lambda \times \log(P_\lambda)\, d\lambda \end{cases} \quad (8)$$

3. RESULTS AND DISCUSSION

A healthy human subject was scanned using a singly-refocused 2D single shot spin echo brain EPI sequence at 7 Tesla. Imaging parameters were: FOV: 192x192 mm^2 (matrix: 196x96) to yield a spatial resolution of 2x2x2 mm^3, TR/TE 4800/57 ms, and an acceleration factor (GRAPPA) of 2. A 6/8 partial Fourier transform was used along the phase-encoding direction. Diffusion-weighted images were acquired at three *b*-values of 1000, 2000 and 3000 s/mm^2, each with 256 directions, along with 31 baseline (non-diffusion-weighted) images. EPI echo spacing was 0.57 ms, with a 2895 Hz/Px bandwidth. **Figure 2** shows one axial slice of the T2 image and diffusion-weighted images (DWI) for the three different shells. The visualization of DWI from

each of the three shells indicated that, as expected, the SNR decreases as *b*-value increases.

Figure 3 visualizes the GFA calculated from the single shells and from the combined multi-shell data. Simple paired *t*-tests show that GFA values increase with increasing *b*-value for single shells, and multi-shell HARDI (with staggered angular sampling; LS Multi-shell-2 mode) achieves the highest GFA values compared to any single-shell HARDI dataset and compared to multi-shell with consistent angular sampling in every shell (LS Multi-shell-1 mode).

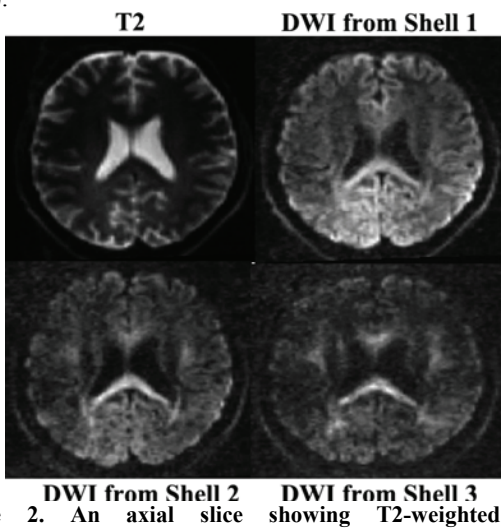

Figure 2. An axial slice showing T2-weighted and corresponding three single-shell HARDI diffusion-weighted images (DWI). Estimated SNR values for the three shells are 11.2 (shell 1), 6.6 (shell 2) and 6.3 (shell 3).

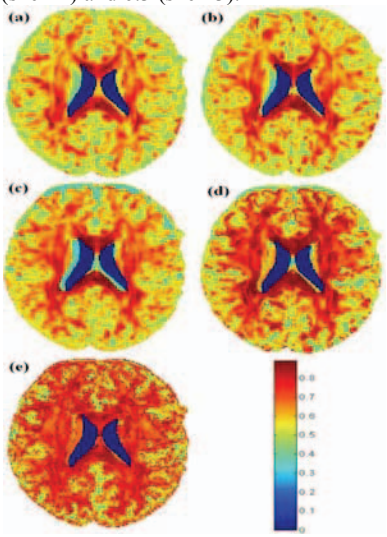

Figure 3. GFA calculated from single-shell and multi-shell HYDI as in Figure 2. (a) GFA calculated from Shell 1 (*b*=1000 s/mm^2), (b) GFA calculated from Shell 2 (*b*=2000 s/mm^2), (c) GFA calculated from Shell 3 (*b*=3000 s/mm^2). (d) GFA calculated from LS Multi-shell mode 1 (fixed angular sampling) and (e) GFA calculated from mode 2 (staggered angular sampling). The multi-shell data correctly show the higher GFA and high contrast in the cortical U-fibers, which tend to have partial voluming with gray matter and CSF. In the plot, CSF was removed using Brainsuite package (http://www.loni.ucla.edu/Software/BrainSuite).

Figure 4 shows three entropy measures for the 3 single-shell datasets and for the combined multi-shell HARDI human brain data. **Figure 5** also shows mean values of three entropy measures for single shells and multi-shell HYDI, the trend was confirmed by using paired *t* tests. As shown in **Figures 4 and 5**, a higher *b*-value provides more information for estimating fiber tract orientation (i.e., lower entropy; *column 2* of **Figure 5**), but less information for estimating their eigenvalues (i.e., higher entropy, *column 3* of **Figure 5**). Combining both components, *b*=1000 provides the best overall information content (lowest entropy), as shown in *column 1* of **Figure 5**. Moreover, we noticed a substantial information gain by combining all single-shell HARDI into one multi-shell HARDI. This is shown by the entropy decreases in all three columns of **Figure 5** for the multi-shell data.

To explain this differential information content, we reasoned that a higher *b*-value leads to an overall decrease in the magnitude of diffusion-weighted signals, except for those acquired along gradient directions orthogonal to the fiber orientations, thus allowing a better determination of the fiber orientation. To provide an intuitive understanding, it may help to consider the extreme case of diffusion-weighted images acquired at an infinite *b*-value, in which the diffusion-weighted signals are zero except for those gradient directions exactly orthogonal to the main fiber orientations. In such case, there is no data for us to estimate the eigenvalues and thus no intrinsic information exists (i.e., infinite uncertainty) with respect to the eigenvalue component.

4. CONCLUSION

In this paper, we showed how varying the *b*-value affects the achievable accuracy when estimating fiber orientations and fiber eigenvalues in HARDI reconstruction. In the range we studied (1000-3000 s/mm^2), a higher *b*-value provided more information for estimating fiber orientations. This comes at the expense of losing some accuracy when estimating its corresponding eigenvalues. HARDI data collected with multiple shells thus outperforms its single-shell counterpart by including shells acquired at both low and high *b*-values. Moreover, staggered angular sampling in different shells can achieve better results than a fixed angular sampling in multi-shell HARDI. In future, adaptive weighting strategy multi-shell HYDI will be investigated and its' effect on fiber tractography will be studied.

Acknowledgments:
This project was funded by NIH grants R01 EB008432 and EB007813, partly funded by P41 RR008079, P30 NS057091 and the University of Minnesota Institute for Translational Neuroscience.

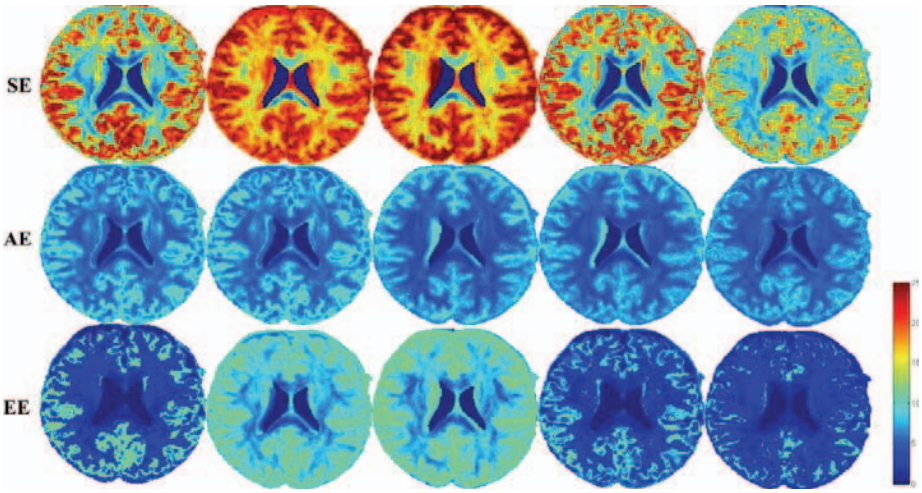

Figure 4. Entropy comparisons for different single shell acquisition schemes and multi-shell HYDI (last two columns). In order from top row to bottom row, show SE, AE and EE in respectively. In order from left column to right column, show data from Shell 1 (b=1000 s/mm^2), Shell 2 (b=2000 s/mm^2), Shell 3 (b=3000 s/mm^2) and LS Multi-shell mode 1 (fixed angular sampling) and mode 2 (staggered angular sampling). In the plot, CSF was removed using Brainsuite package. (http://www.loni.ucla.edu/Software/BrainSuite).

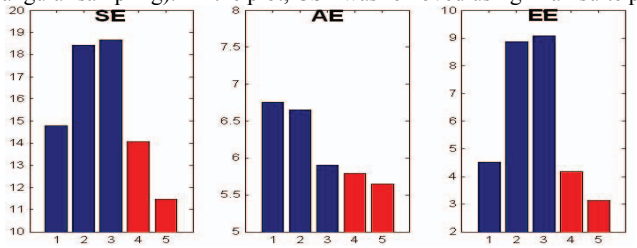

Figure 5. Mean values of 3 entropy measures in WM for the 3 single-shell and the combined multi-shell (mode 1 and 2) HYDI human brain data. (a) SE. (b) AE (c) EE. In each graph, the plotted bars, in the order from left to right, show data for Shell 1, Shell 2, Shell 3 and LS Multi-shell mode 1 (fixed angular sampling) and mode 2 (staggered angular sampling). Simple paired t-tests confirmed statistical significance of these differences at p=0.05. WM was segmented using Brainsuite package.

5. REFERENCES

1. Basser PJ, Pierpaoli C. Microstructural and physiological features of tissues elucidated by quantitative diffusion tensor MRI. **J. Magn. Reson**. vol. B 111, no. 3, pp.209-219 (1996).
2. Le Bihan D. IVIM method measures diffusion and perfusion. **Diagn Imaging** (San Franc). 12(6):133, 136 (1990).
3. Tuch DS, Q-Ball Imaging. **Magnetic Resonance in Medicine** 52:1358-1372 (2004).
4. Alexander DC. Maximum entropy spherical deconvolution for diffusion MRI. In: Proc. **19th Int. Conf. on Info. Processing in Medical Imaging (IPMI)**, Glenwood Springs, CO, USA (2005).
5. Özarslan E, Shepherd T, Vemuri BC, Blackband S, Mareci T. Resolution of complex tissue microarchitecture using the diffusion orientation transform (DOT). **NeuroImage** 31(3): 1083–1106 (2006).
6. Jansons KM, Alexander DC. Persistent angular structure: new insights from diffusion magnetic resonance imaging data. **Inverse Problems** 19: 1031-1046 (2003).
7. Anderson AW. Measurement of fiber orientation distributions using high angular resolution diffusion imaging. **Magn Reson Med**. 54: 1194-1206 (2005).
8. Chiang WY, Tseng WYI, Perng MH (2010). Q-Space Sampling Method and Diffusion Spectrum Imaging Method Employing the Same, US Patent Application, http://www.faqs.org/patents/app/20080272781.
9. Wedeen VJ, Hagmann P, Tseng WI, Reese TG, Weisskoff RM. Mapping complex tissue architecture with diffusion spectrum magnetic resonance imaging. **Magnetic Resonance in Medicine** 54(6):1377–1386 (2005).
10. Khachaturian MH, Wisco JJ, Tuch DS. Boosting the sampling efficiency of q-ball imaging using multiple wavevector fusion. **Magnetic Resonance in Medicine** 57(2):289–296 (2007).
11. Wu YC, Field AS, Alexander AL. Computation of diffusion function measures in q-space using magnetic resonance hybrid diffusion imaging. **IEEE Transactions on Medical Imaging** 27(6):858–865 (2008).
12. Descoteaux M, Deriche R, Le Bihan D, Mangin JF, Poupon C. Diffusion Propagator Imaging: Using Laplace's equation and multiple shell acquisitions to reconstruct the diffusion propagator. In: **Proc. of the 21st Intl. Conf. on IPMI**; Williamsburg, VA, USA (2009).
13. Leow AD, Zhu S, Zhan L, McMahon K, de Zubicaray GI, Meredith M, Wright MJ, Toga AW, Thompson PM. The tensor distribution function. **Magn Reson Med**. 2009 Jan;61(1):205-14.
14. Descoteaux M, Angelino E, Fitzgibbons S, Deriche R. Regularized fast and robust analytical Q-ballimaging. **Magn Reson Med** 58:497–510 (2007).
15. Aganj I, Lenglet C, Sapiro G, Yacoub E, Ugurbil K & Harel N. Reconstruction of the orientation distribution function in single and multiple shell q-ball imaging within constant solid angle. **Magnetic Resonance in Medicine**, vol. 64, no. 2, pp. 554-566, 2010.
16. Zhan L, Leow AD, Jahanshad N, Chiang MC, Barysheva M, Lee AD, Toga AW, McMahon KL, de Zubicaray GI, Wright MJ, Thompson PM. How does angular resolution affect diffusion imaging measures? **Neuroimage**. 2010 Jan 15;49(2):1357-71. Epub 2009 Oct 9.